J. T. K. L.
JURNAL TEKNIK KIMIA DAN LINGKUNGAN

J. Tek. Kim. Ling. 2026, 10 (1), 55-74
p-ISSN : 2579-8537, e-ISSN : 2579-9746
http://jurnal.polinema.ac.id/index.php/jtkl
DOI: http://dx.doi.org/10.33795/jtkl.v10i1.8795

Hybrid Composite of Biomass-Derived Activated Carbon and Mg/Al Hydrotalcite for Caffeine Adsorption from Aqueous Solutions

Estin Nofiyanti*, Noer Laelly Barorroh Taufik Abdul Ghofur, Dian Utami

[1]Program Study of Environmental Engineering, Universitas Muhammadiyah Tasikmalaya, Tamansari Street KM. 2, Tasikmalaya City 46196, Indonesia

ABSTRACT

This study investigated the adsorption performance of activated carbon (AC) derived from jengkol (*Pithecellobium jiringa*) peel and its composites with Mg/Al hydrotalcite (HT) for caffeine removal from aqueous solutions. The adsorbents were characterized using FTIR, XRD, and SEM-EDX, confirming the presence of –OH groups, M–O–M bonding, and layered porous morphology. Batch adsorption experiments evaluated the effects of contact time, pH, and initial concentration. AC showed the highest removal efficiency (96.44% at 3 ppm), while ACHT 12 demonstrated stable performance at moderate concentrations and fit well to the Langmuir isotherm (R^2 = 0.9609) and pseudo-second-order kinetics (R^2 = 0.9912). ACHT 21 followed the Freundlich model (R^2 = 0.7758), indicating heterogeneous multilayer adsorption. Optimal adsorption occurred in acidic conditions (pH 3–5), which reflects the characteristics of pharmaceutical wastewater. The results confirm the potential of jengkol-based adsorbents as low-cost, sustainable alternatives for caffeine-contaminated water treatment.

Keywords: adsorption, caffeine, isotherm, jengkol peel, kinetics.

1. INTRODUCTION

The increasing presence of caffeine in Indonesian wastewater, with concentrations reported up to 12 µg/L from household and hospital sources, underscores its status as an emerging contaminant of ecological and public health concern. Entry into wastewater primarily occurs through human excretion, with about 10% of ingested caffeine eliminated in urine and feces [1,2], while additional inputs arise from the widespread consumption of coffee, tea, energy drinks, and pharmaceutical products [3,4], as well as from hospital use, particularly in neonatal and pediatric care for treating apnea of prematurity [5,6]. The persistence of caffeine even after conventional treatment [6,7] highlights inefficiencies in removal processes, raising concerns about its ecological impacts, including disruption of microbial communities, altered behavior of aquatic organisms, and trophic-level imbalances [8,9]. Moreover, its stability in the environment, with a half-life of 100–240 days [10,11], suggests potential accumulation and long-term risks to aquatic ecosystems. From a public health perspective, the detection of caffeine in drinking water sources reliant on surface waters contaminated by wastewater discharges [12,13] raises further concerns, as caffeine often co-occurs with Pharmaceuticals and Personal Care Products (PPCPs), indicating broader pollution loads [11]. Consequently, the rising concentrations of caffeine in Indonesian wastewater not only reflect societal patterns of consumption and disposal but also emphasize the urgent need for improved monitoring, regulatory measures, and advanced treatment technologies to mitigate its ecological and public health impacts.

The persistence of caffeine in aquatic environments, mainly due to its resistance to conventional wastewater treatment, combined with its ecotoxicological effects and frequent coexistence with antibiotics and Antibiotic Resistance Genes (ARGs),

*Corresponding author:
E-mail: estin.nofi@umtas.ac.id (Estin Nofiyanti)
How to cite: Nofiyanti, et al., Jurnal Teknik Kimia dan Lingkungan 10 (2026) 55–74.

Submitted : September 15, 2025
Revised : February 23, 2026
Accepted : February 25, 2026

presents a complex public health concern. Although often labelled a "labile" contaminant, caffeine has been reported in concentrations up to 240 µg/L in untreated wastewater and persists in aquatic systems because removal efficiencies of traditional treatments, such as sedimentation or biological filtration, are often limited to 20–30% [12,14]. Its high solubility and low volatility contribute to its environmental stability, enabling accumulation not only in water bodies but also in sediments [15]. Ecotoxicological evidence shows that exposure to caffeine can disrupt metabolic processes, impair growth and reproductive success, and increase oxidative stress in aquatic organisms, ultimately leading to population declines, altered community structures, and reduced ecosystem resilience [16–18]. These physiological disruptions weaken aquatic organisms' defenses, elevating susceptibility to disease and mortality. More critically, caffeine often coexists with antibiotics in wastewater, facilitating localized toxicity while also creating conditions conducive to horizontal transfer of ARGs among microbial communities, thereby promoting antimicrobial resistance [12,19–21]. This interconnectedness between environmental contamination and human health highlights how the persistence of caffeine and its synergistic interactions with other pollutants reinforce the cycle of ecological disruption and antibiotic resistance, emphasizing the urgent need for advanced wastewater treatment innovations and robust monitoring strategies to mitigate the environmental and public health risks posed by emerging contaminants.

In response to this problem, adsorption has emerged as a simple, cost-effective, and scalable technique for removing organic micropollutants from wastewater. The comparative effectiveness of Activated Carbon (AC) and Mg/Al Hydrotalcite (HT) for removing polar organic micropollutants such as caffeine depends on their adsorption mechanisms, efficiency, surface area, and mechanical stability. Activated carbon, with its extensive surface area (300–1000 m^2/g) and porous structure, achieves high adsorption efficiencies through predominantly physisorption with possible chemisorption depending on contaminant characteristics and operational conditions such as pH and temperature [22–25]. In contrast, HT adsorb pollutants primarily via anion-exchange mechanisms and complexation, showing effectiveness against contaminants like nitrophenols but with limitations linked to their relatively low surface area and weaker mechanical stability in aqueous environments [26,27]. While AC exhibits strong structural integrity, enabling repeated use in fixed bed systems, HT are prone to structural collapse or leaching under ion exchange or dissolution conditions, which restricts their large-scale applicability [25,26]. Although both materials can remove caffeine and other polar micropollutants, activated carbon generally outperforms hydrotalcites in terms of adsorption capacity, efficiency, and durability, making it more practical for wastewater treatment unless economic or site-specific factors justify alternative use.

Hybrid adsorbents combining biomass-derived AC with HT represent a sustainable and low-cost solution for wastewater treatment, particularly in decentralized systems such as those in Indonesia. AC provides high surface area and porosity for effective adsorption of polar organic micropollutants, while HT contributes ion exchange capacity and structural stability, creating a synergistic mechanism that enhances removal efficiency, often exceeding 90% [28,29]. Using agricultural residues as AC precursors not only reduces costs but also supports circular economy principles by repurposing waste [30]. In this context, the utilization of locally available biomass such as jengkol (*Pithecellobium jiringa*) peel offers a distinctive environmental advantage. It transforms abundant agricultural waste into a value-added material, minimizing solid waste accumulation and reducing the carbon footprint associated with conventional

adsorbent production. This dual-action approach improves resilience under variable pH and temperature, making hybrid adsorbents practical for rural and community-based wastewater systems lacking centralized infrastructure [31]. Furthermore, employing indigenous biomass sources aligns with national sustainability goals and empowers local communities through resource valorization and environmentally conscious innovation.

The objective of this study is to synthesize and characterize a hybrid adsorbent material using FTIR, XRD, SEM-EDX, and SAA techniques, and to evaluate its performance in removing caffeine from aqueous media under various conditions. The outcomes are expected to provide insights into the development of efficient adsorbents based on local resources, contributing to national goals in water quality improvement and pollution reduction in accordance with Sustainable Development Goals (SDG 6.3).

2. RESEARCH METHODS

This study was conducted through five main stages: (1) preparation of activated carbon from jengkol peel biomass, (2) synthesis of Mg/Al Hydrotalcite (HT), (3) fabrication of the composite material, (4) characterization, and (5) adsorption testing of caffeine from aqueous solutions.

2.1. Preparation of Activated Carbon

Jengkol peels were collected, washed thoroughly with distilled water, and dried in the sunlight for 48 hours. The dried biomass was carbonized in a furnace at 450°C for 40 minutes. The resulting charcoal was soaked in a 15% H_3PO_4 solution for 24 hours to activate the surface, then rinsed with distilled water until a neutral pH was reached. The sample was dried at 105°C for 3 hours and ground into powder.

2.2. Synthesis of Mg/Al Hydrotalcite

The HT was synthesized using the co-precipitation method. A solution of $Mg(NO_3)_2 \cdot 6H_2O$ (0.5 M) and $Al(NO_3)_3 \cdot 9H_2O$ (0.25 M) was mixed in a molar ratio of 2:1. While stirring continuously under a nitrogen atmosphere, 1 M NaOH was added dropwise to maintain the pH at 10±0.5. The resulting slurry was aged for 24 hours, filtered, washed with distilled water, and dried at 70°C.

2.3. Composite Formation and Characterization

AC and HT were mixed in different mass ratios (1:1 (ACHT 11), 1:2 (ACHT 12, and 2:1 (ACHT 21)) and stirred in 100 mL of deionized water for 24 hours at room temperature. The mixture was filtered, dried at 105°C for 6 hours, and sieved to obtain a homogeneous composite powder. The samples were characterized using Fourier Transform Infrared Spectroscopy (FTIR), X-Ray Diffraction (XRD), Scanning Electron Microscopy with Energy Dispersive X-ray (SEM-EDX), and Surface Area Analyzer (SAA) to examine functional groups, crystalline structure, elemental composition, and surface morphology.

2.4. Adsorption Test

Adsorption experiments were conducted to evaluate the caffeine removal efficiency of the synthesized composites. A stock solution of caffeine was prepared by dissolving analytical grade caffeine powder in distilled water. All batch adsorption tests were carried out using 50 mg of adsorbent and 10 mL of caffeine solution under controlled agitation at room temperature.

Kinetic studies were performed by varying the contact time between 1 and 50 minutes while maintaining a fixed initial caffeine concentration. Samples were withdrawn at regular intervals, filtered, and analyzed using a UV-Vis spectrophotometer at 273 nm. The kinetic data were fitted to pseudo-first-order and pseudo-second-order models to determine the adsorption mechanism.

Isotherm studies were carried out by varying the initial concentration of caffeine from 1 to 13 ppm with a fixed adsorbent dosage. The equilibrium data were fitted to the Langmuir and the Freundlich isotherm models to assess

the adsorption capacity and surface characteristics.

The effect of pH on caffeine adsorption was investigated by adjusting the solution pH to 3, 5, 7, 9, and 11 using 0.1 M HNO_3 or 0.1 M NaOH. The optimal pH for maximum adsorption efficiency was determined by comparing the removal percentages across different pH values.

3. RESULTS AND DISCUSSION

3.1. Characterization of Adsorbent Materials

Characterization was carried out to confirm the successful synthesis and modification of adsorbent materials based on activated carbon derived from jengkol peel, composited with HT. The analytical techniques employed included FTIR to identify functional groups, XRD to assess crystallinity, SEM–EDX to observe surface morphology and elemental distribution, and SAA to determine surface area and pore distribution. These methods were used in combination to evaluate the physicochemical properties and structural integrity of the materials for environmental adsorption applications.

FTIR spectroscopy plays a crucial role in identifying functional groups and monitoring structural transformations in biomass-derived activated carbon, with key peaks reflecting the evolution of organic functionalities during carbonization (Figure 1). A broad absorption band around ~3444 cm^{-1} corresponds to O–H stretching vibrations, confirming the presence of hydroxyl groups that may originate from residual moisture or activation agents, which enhance adsorption by improving interactions with polar molecules in aqueous systems [32]. Another notable feature is the peak near ~1620 cm^{-1}, attributed to aromatic C=C stretching, indicating the formation of aromatic domains and sp^2 hybridized carbon structures during pyrolysis, which contribute to stability and adsorption capacity. Additionally, the disappearance of bands in the 1800–1500 cm^{-1} region signifies the decomposition of unstable organic groups and the removal of volatile compounds, leading to the enrichment of the carbon matrix with more stable configurations [33].

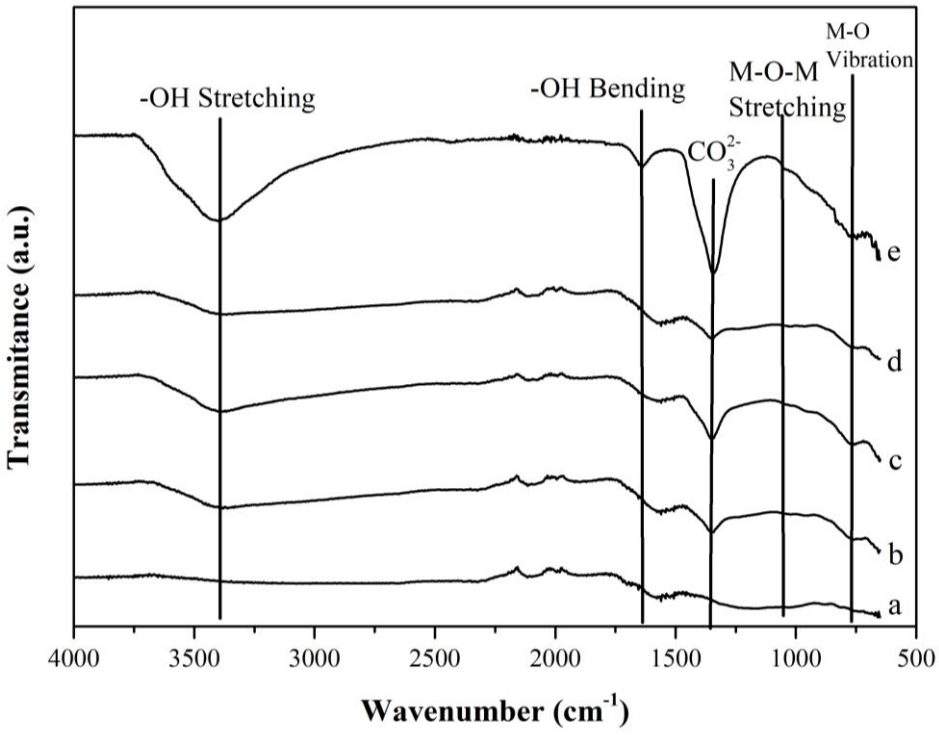

Figure 1. FTIR spectra of (a) activated carbon from jengkol peel (AC), (b) composite ACHT 11, (c) ACHT 12, (d) ACHT 21, and (e) HT.

FTIR spectroscopy provides crucial insights into the structural integrity and functional characteristics of ACHT composites, particularly through the identification of key absorption bands such as carbonate (~1345 cm^{-1}), metal–oxygen (~760 cm^{-1}), and aromatic C=C (~1620 cm^{-1}). The persistence of the carbonate band demonstrates that hydrotalcite structures remain intact within the composite, with carbonate ions stabilizing the Mg^{2+}/Al^{3+} brucite-like layers and supporting ion-exchange and redox activity essential for contaminant removal [34]. Similarly, the retention of metal–oxygen (M–O) vibrations at ~760 cm^{-1} confirms the presence of metal hydroxide groups typical of layered double hydroxides, ensuring the stability of HT in the composite matrix [35]. Meanwhile, the aromatic C=C stretching peak at ~1620 cm^{-1} indicates the contribution of activated carbon, providing π–π stacking sites for interactions with aromatic organic pollutants [36]. Collectively, these spectral signatures highlight the successful integration of both organic and inorganic functionalities within the hybrid adsorbent.

The functionalities identified in the FTIR spectra directly contribute to multiple adsorption mechanisms that enhance wastewater treatment performance. Carbonate and M–O groups promote ion exchange, improving the removal of ionic species such as heavy metals and anions [34], while hydroxyl groups associated with the metal hydroxide phase facilitate hydrogen bonding with polar contaminants [37]. Additionally, the intrinsic charge of HT layers supports electrostatic interactions with negatively charged pollutants, further enhancing anion capture [35]. At the same time, the aromatic domains from activated carbon enable π–π stacking with organic micropollutants, significantly improving adsorption affinity for aromatic and unsaturated compounds [36].

XRD analysis of biomass-derived activated carbon typically shows a broad amorphous peak at ~2θ ≈ 23° (Figure 2), confirming its disordered carbon structure and low crystallinity. Unlike sharp peaks that indicate graphitic order, this broad feature reflects structural disorder formed during biomass carbonization [38–40]. Such amorphous characteristics are advantageous for wastewater treatment, as they enhance surface area, functional group accessibility, and reactivity, thereby improving adsorption performance. The disordered framework facilitates diverse mechanisms, including hydrogen bonding, electrostatic interactions, and ion exchange with polar contaminants and ionic toxins [41,42].

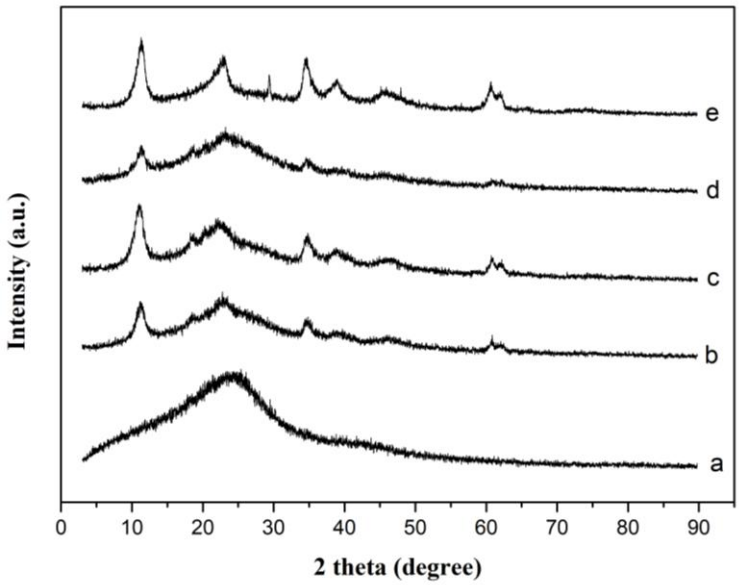

Figure 2. XRD patterns of (a) AC, (b) ACHT 11, (c) ACHT 12, (d) ACHT 21, and (e) HT.

XRD analysis is essential for confirming the structural integrity of HT and assessing the impact of varying AC to HT ratios in hybrid composites. Characteristic HT peaks typically appear at 2θ ≈ 11.6°, 23.3°, 34.7°, 39.3°, 46.8°, and 60.8°, consistent with JCPDS No. 54-1030, reflecting the ordered layered double hydroxide (LDH) structure and confirming the stable arrangement of Mg^{2+} and Al^{3+} ions during composite formation [35,43]. Increasing the proportion of activated carbon generally reduces the intensity and sharpness of these peaks, indicating dilution of the HT phase, reduced crystallinity, and partial introduction of amorphous features from carbon [44,45]. Such structural changes influence ion exchange capacity, as lower crystallinity reduces available interlayer sites, though a balanced AC:HT ratio can optimize both ion exchange from HT layers and high surface area contributions from carbon, enhancing adsorption performance [46,47].

SEM provides valuable insights into the morphology, porosity, and structural characteristics of biomass-derived AC and its composites with HT. As shown in Figure 3.a, the AC sample exhibits a porous, rough, and layered morphology with numerous cavities, confirming its high surface area and suitability for adsorption applications [45]. In the composites, ACHT 11 (Figure 3.b) and ACHT 12 (Figure 3.c) display partial surface coverage by aggregated HT platelets, indicating successful deposition of HT onto the carbon matrix [36], with ACHT 12 showing a denser HT phase compared to ACHT 11. By contrast, ACHT 21 (Figure 3.d) reveals weaker HT features and a more dominant carbon morphology, consistent with a higher AC:HT ratio.

These observations highlight that varying HT content alters surface coverage and structural balance, as higher HT loadings improve ion exchange potential but may reduce exposed carbon surface area [48], while higher AC content enhances porosity but decreases crystallinity of the HT phase [49]. SEM analysis confirms that the hybrid composites retain the dual functionalities of AC and HT, with morphology tuned by the AC:HT ratio to optimize adsorption and ion-exchange properties for wastewater treatment applications [50].

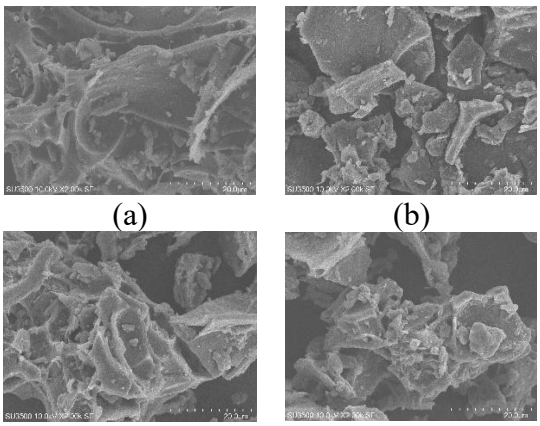

Figure 3. SEM micrographs of (a) AC, (b) ACHT 11, (c) ACHT 12, and (d) ACHT 21 at 2000× magnification.

The EDX results (Table 1) supported these morphological observations. The AC sample was primarily composed of carbon (78.51%) and oxygen (18.47%), with a trace of chlorine (3.02%), likely residual from the activation process [51]. ACHT 11 exhibited high contents of Mg (27.90%) and Al (16.18%), with carbon content decreasing to 4.94%, indicating extensive HT presence [52]. In contrast, ACHT 12 and ACHT 21 had higher carbon content (~55%) but still retained detectable amounts of Mg and Al, suggesting that HT was incorporated but in lower proportions [53]. The appearance of Na (1.86%) in ACHT 12 likely originated from residual NaOH used during HT synthesis [54].

Table 1. Elemental composition (wt%) of AC and ACHT composites obtained from EDX analysis.

Sample	C (%)	O (%)	Mg (%)	Al (%)	Na (%)	Cl (%)
AC	78.51	18.47	-	-	-	3.02
ACHT 11	4.94	50.98	27.90	16.18	-	-
ACHT 12	55.66	35.71	4.34	2.44	1.86	-
ACHT 21	54.82	34.57	7.72	2.90	-	-

SEM–EDX results confirmed the successful hybridization of the organic–inorganic phases and highlighted that the AC:HT ratio significantly affects surface coverage and elemental distribution. These hybrid materials combine the high surface area of activated carbon with the ion exchange and electrostatic properties of HT, offering synergistic performance for the adsorption of both organic and ionic contaminants in water. Activated carbon plays a crucial role in adsorption due to its well-developed pore structure, characterized by a large specific surface area, pore volume, and pore-size distribution. However, surface modification can alter these characteristics and significantly affect adsorption performance. Consistent with the data in Table 2, the modification of AC to ACHT resulted in a decrease in the specific surface area from 46.626 m2/g to 12.029–18.728 m^2/g. This indicates that some of the micropores are closed or filled by the modified phase [55]. On the other hand, the pore volume of ACHT increased from 0.009 cc/g in AC to 0.018-0.020 cc/g, accompanied by an increase in the pore radius from 26.415 Å to 26.881–27.112 Å, indicating a pore restructuring from predominantly micropores to predominantly mesopores. This phenomenon is caused by surface modifications that do not always result in an increase in the specific surface area, but can also enlarge the pore size and volume due to the restructuring of the carbon framework or the deposition of new phases on the pore surface [56]. These changes in pore characteristics have implications for the adsorption mechanism. Although the surface area of ACHT is lower, the increase in pore volume and size can increase the diffusivity and accessibility of medium to large molecular weight adsorbates into the pore structure, so that adsorption performance is not solely determined by the specific surface area, but also by the distribution and effective pore volume [55,56].

Table 2. Surface area and pore distribution of AC and ACHT.

Sample	Surface Area (m^2/g)	Pore Volume (cc/g)	Pore radius (Å)
AC	46.626	0.009	26.415
ACHT 11	12.529	0.018	27.017
ACHT 12	12.029	0.019	27.112
ACHT 21	18.728	0.02	26.881

3.2. Effect of Contact Time and Adsorption Kinetics

The adsorption performance of the synthesized materials was first evaluated by examining the effect of contact time on caffeine removal (Figure 4). All adsorbents demonstrated a rapid increase in adsorption percentage within the first 10 minutes, followed by a slower rate until equilibrium was reached at approximately 50 minutes [57,58]. This kinetic behavior reflects the initial abundance of active sites that gradually became saturated over time. Among the tested materials, AC exhibited the highest adsorption capacity, reaching about 55% at equilibrium [59], which can be attributed to its microporous and mesoporous structure that facilitates caffeine diffusion and provides a large surface area for adsorption [57]. In comparison, the

composite materials (ACHT 11, ACHT 12, and ACHT 21) showed slightly lower but still competitive adsorption performance, indicating that hydrotalcite modification alters surface properties and pore structures while maintaining effective adsorption [60,61].

To further elucidate the adsorption mechanism, kinetic modelling was conducted using the pseudo-first order model (Santosa–Muzakky) for AC and the pseudo-second order model (Ho–McKay) for the composites. The best-fitting model was determined based on the highest coefficient of determination (R^2), and the resulting parameters are presented in Table 3.

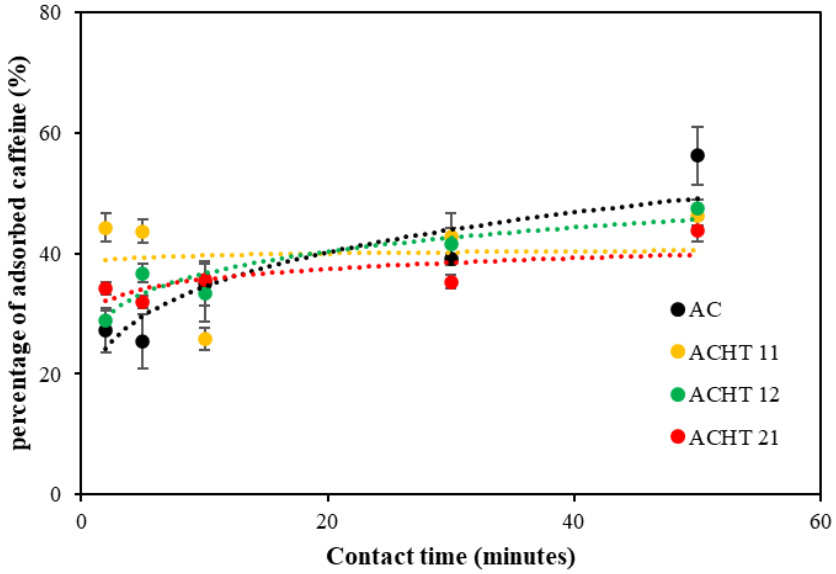

Figure 4. Effect of contact time on caffeine adsorption percentage by various adsorbents.

Table 3. Adsorption Kinetics Parameters.

Adsorbent	Kinetic Model	R^2	q_e (mg/g)	K (g/mg.min)	Adsorption Mechanism Interpretation
AC	Santosa-Muzakky (pseudo 1st)	0.9664	-	0.0045	Film diffusion and surface-level physical interactions
ACHT 11	Ho-McKay (pseudo 2nd)	0.9725	0.9560	3.2796	Chemisorption with moderate capacity and rate
ACHT 12	Ho-McKay (pseudo 2nd)	0.9912	0.9731	2.9980	Highest adsorption capacity among composites
ACHT 21	Ho-McKay (pseudo 2nd)	0.9812	0.8660	3.3050	Fastest adsorption rate with moderate capacity

3.3. Adsorption Isotherm Models

The effect of initial caffeine concentration on adsorption efficiency was investigated over the range of 3 to 11 ppm using four types of adsorbents (AC, ACHT 11, ACHT 12, and ACHT 21). All materials showed a decreasing trend in adsorption percentage as the initial concentration increased (Figure 5). For example, AC exhibited the highest adsorption efficiency of 96.44% at 3 ppm, which declined to 42.34% at 11 ppm. A similar pattern was observed for ACHT 12 (from 89.82% to 42.53%), ACHT 21 (from 33.84% to 42.41%), and ACHT 11 (from 18.29% to 51.34%). The decline in caffeine adsorption percentage at higher concentrations is primarily attributed to the saturation of active sites on the adsorbent surface. At low concentrations, a high ratio of available sites to solute molecules promotes efficient adsorption. However, as solute concentration increases, active sites become increasingly occupied, reducing adsorption efficiency, even though the total mass

adsorbed may continue to rise [62,63]. This saturation phenomenon is well documented across various systems, including dye and methane adsorption, where site saturation diminishes per site effectiveness [64–66]. Additionally, increasing adsorbent dosage may initially improve surface availability, but eventually leads to reduced capacity due to site crowding [62].

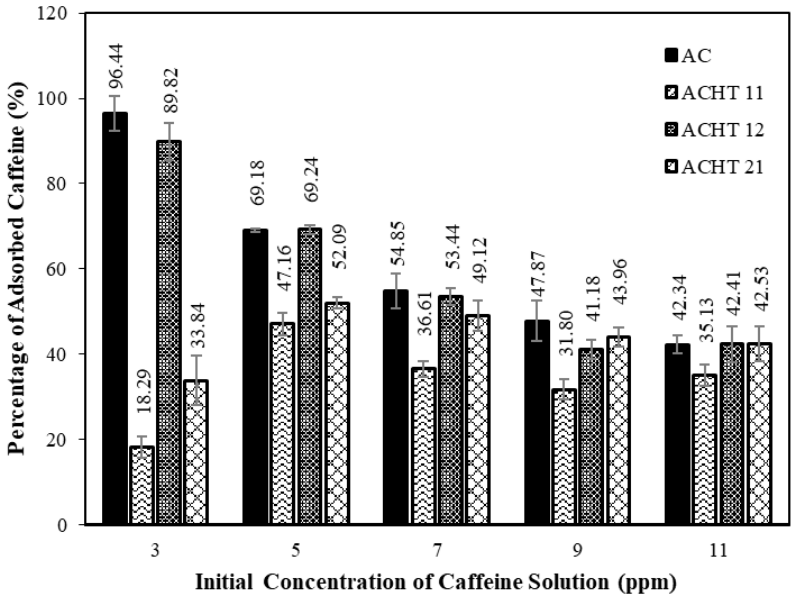

Figure 5. Effect of initial caffeine concentration on the percentage of caffeine adsorbed by various adsorbent at 50 minutes contact time.

To further understand the adsorption mechanism, equilibrium data were analyzed using the Langmuir and the Freundlich isotherm models, with the calculated parameters presented in Table 4. The coefficient of determination (R^2) served as the goodness-of-fit indicator, and the caffeine adsorption onto AC and ACHT 12 showed the best fit with the Langmuir model, yielding R^2 values of 0.9861 and 0.9609, respectively. This strong correlation suggests monolayer adsorption on a homogeneous surface with uniform adsorption energy. The applicability of the Langmuir model for caffeine adsorption onto activated carbon-based materials has also been reported in prior studies, where high R^2 values similarly indicated the presence of energetically uniform adsorption sites and the absence of significant adsorbate-adsorbate interactions [67,68]. While several supporting studies focus on other adsorbates such as dyes or heavy metals [69,70], they reinforce the broader reliability of the Langmuir model in predicting monolayer adsorption. However, direct validation using caffeine-specific systems remains essential to avoid misinterpretation and ensure model relevance [69,70].

In contrast, caffeine adsorption onto ACHT 11 and ACHT 21 was better described by the Freundlich model, with R^2 values of 0.5797 and 0.7758, respectively. It indicates adsorption on a heterogeneous surface and potentially multilayer formation. The Freundlich constant n values for all adsorbents exceeded 1, indicating favorable adsorption conditions [71].

Based on the Langmuir model analysis, the maximum adsorption capacity (q_{max}) was determined to be 0.9652 mg/g for AC and 0.8991 mg/g for ACHT 12, both of which are significantly higher than those of the other synthesized composites. The highest Freundlich constants (K_F) were also recorded for AC (0.7171) and ACHT 21 (0.6403), corroborating the results shown in Figure 5. These adsorption capacity values can be

categorized as relatively low compared to those of nanoporous carbons or chemically activated adsorbents reported in recent literature, which generally exhibit adsorption capacities ranging from 1.5 to 4 mg/g due to their high specific surface areas and well-developed microporous structures [72]. Nevertheless, the q_{max} values obtained in this study remain comparable to several biomass-derived carbons prepared through mild chemical activation, particularly considering variations in activation methods and the nature of the biomass precursor used.

Several studies have demonstrated that certain biomass-derived materials can indeed process adsorption capacities below 0.9 mg/g. For instance, sunflower husk biochar and goethite exhibited adsorption capacities of 0.64 mg/g and 0.52 mg/g, respectively, for specific contaminants such as carboxin and diuron [73]. Similarly, vinegar-residue biochar exhibited a maximum adsorption capacity of only 2.91 mg/g toward cadmium ions [74], underscoring the significant variability in the performance of biomass-derived materials, which depends on their specific application context. Conversely, modification or further activation processes can substantially enhance performance. For example, biochar from Fenton sludge achieved phosphorus adsorption capacities up to 68.49 mg/g [75]. In this context, the material developed in this study, which underwent chemical activation (with HNO_3), displayed moderate q_{max} values likely due to partial pore blockage by HT particles and the predominance of mesoporous rather than microporous structures, which limited caffeine accessibility to the active sites.

On the other hand, numerous reports have documented significantly higher adsorption capacities for strongly activated biomass carbons and nanoporous carbon derivatives. Adsorption capacities exceeding 200 mg/g for various organic pollutants and heavy metals have been reported for biomass-derived activated carbons [76]. Adsorption capacities of 214– 217 mg/g for diclofenac and 260– 275 mg/g for paroxetine have also been observed in studies of activated carbon from argan shells [77]. Furthermore, biomass-derived carbons with high ion-storage capacities, ranging from 192 to 618 mAh/g, have been documented in recent work [78], indicating exceptional surface area and ion-interaction potential. Therefore, although the q_{max} values obtained here are moderate, the ACHT composite system offers a balanced compromise between adsorption efficiency, structural stability, and environmental sustainability, making it a promising and practical candidate for decentralized wastewater treatment applications.

Table 4. Langmuir and Freundlich isotherm model parameters for caffeine adsorption onto different adsorbent materials.

Adsorbate	Model	R^2	q_{max} (mg/g)	K_L (L/mg)	b (L/mg)	n
AC	Langmuir	0.9861	0.9652	2.4152	-	-
	Freundlich	0.8959	-	-	0.7171	8.9365
ACHT 11	Langmuir	0.1164	negative	negative	-	-
	Freundlich	0.5797	-	-	0.0802	0.8672
ACHT 12	Langmuir	0.9609	0.8991	2.2542	-	-
	Freundlich	0.8623	-	-	0.6403	6.7431
ACHT 21	Langmuir	0.0288	negative	negative	-	-
	Freundlich	0.7758	-	-	0.1488	0.9433

3.4. Thermodynamic Study of Caffeine Adsorption

Thermodynamic parameters were calculated to evaluate the spontaneity and energetic nature of the interactions between caffeine molecules and the adsorbent surface. The standard Gibbs free energy change ($\Delta G°$) was derived from the equilibrium constant obtained from the Langmuir model (K_L), which was converted to a dimensionless form ($K°$) based on the molar mass of caffeine (194.19 g.mol^{-1}), using Equation 1 [79]:

$$\Delta G° = -RT \ln K° \quad (1)$$

Where: $R = 8.314$ J.mol^{-1}.K^{-1}

$T = 298$ K

The equilibrium constant $K°$ was determined by converting K_L (L·mg^{-1}) to L·mol^{-1} and normalizing it to a standard concentration of 1 mol·L^{-1}. This approach was selected because the calculation of $\Delta G°$ does not require temperature variation, unlike $\Delta H°$ and $\Delta S°$, which must be obtained from multi-temperature isotherms to produce reliable data through the van't Hoff plot. Since this study was conducted at a single temperature (298 K), $\Delta H°$ and $\Delta S°$ were not calculated.

The calculated $\Delta G°$ values for AC and ACHT 12 were −6.25 kJ·mol^{-1} and −6.07 kJ·mol^{-1}, respectively. These negative values indicate that the adsorption process is spontaneous and primarily governed by physisorption, driven by weak van der Waals forces and π–π stacking interactions between the aromatic rings of caffeine and the oxidized carbon surface. The obtained $\Delta G°$ values are consistent with those previously reported for biomass-derived carbon and HT composites, typically ranging between −4 and −7 kJ·mol^{-1} [80,81]. In contrast, negative K_L values obtained for ACHT 11 and ACHT 21 suggest a physically invalid Langmuir regression, likely due to excessive surface heterogeneity or dominance of the hydrotalcite phase, which reduced the affinity for caffeine molecules. Therefore, $\Delta G°$ was only calculated for samples that showed a valid isotherm fit (AC and ACHT 12).

Based on thermodynamic evaluation, the ACHT 12 composite exhibited the most favorable performance compared with pure AC and other composites. Although both materials showed similar $\Delta G°$ values, ACHT 12 demonstrated higher structural stability, better isotherm correlation ($R^2 > 0.96$), and greater regeneration potential. The presence of the hydrotalcite layer in ACHT 12 contributes to surface charge balancing, preventing carbon particle agglomeration and maintaining adsorption efficiency over a broader pH range. In contrast, pure AC tends to exhibit decreased adsorption capacity after several regeneration cycles due to its tightly microporous structure. Therefore, from a thermodynamic and material stability perspective, ACHT 12 can be considered the most promising composite for sustainable caffeine removal, as it effectively balances spontaneity, energy efficiency, and regeneration capability.

3.5. Effect of pH on Caffeine Adsorption

The pH of the solution plays a crucial role in determining adsorption efficiency, as it influences both the surface charge of the adsorbent and the ionization State of the caffeine molecules. The percentage of caffeine adsorbed onto AC, ACHT 11, ACHT 12, and ACHT 21 was evaluated at initial pH values of 3, 5, 7, 9, and 11 (Figure 6). In general, adsorption performance exhibited a strong dependence on pH. AC achieved the highest adsorption efficiency at pH 9, with 76.15%. At the same time, the hydrotalcite-based composites demonstrated optimal performance in acidic conditions, with adsorption percentages of 62.24% for ACHT 11, 71.34% for ACHT 12, and 67.82% for ACHT 21.

This difference in behavior can be attributed to variations in surface charge distribution and zeta potential among the materials. For activated carbon, the point of zero charge (pH_{pzc}) typically lies between 6 and 8. At pH values above this range, the deprotonation of surface functional groups, such as hydroxyl and carboxyl groups, results in a negatively charged surface. Because caffeine remains neutral primarily throughout the tested pH range (pKa approximately 14), electrostatic repulsion between the adsorbent and adsorbate is minimal. Under these conditions, π–π stacking and hydrogen bonding predominate, leading to enhanced caffeine adsorption on the hydrophobic surface of AC. This observation explains the improved adsorption efficiency under alkaline conditions, where surface deprotonation and pore accessibility facilitate caffeine diffusion [82–84].

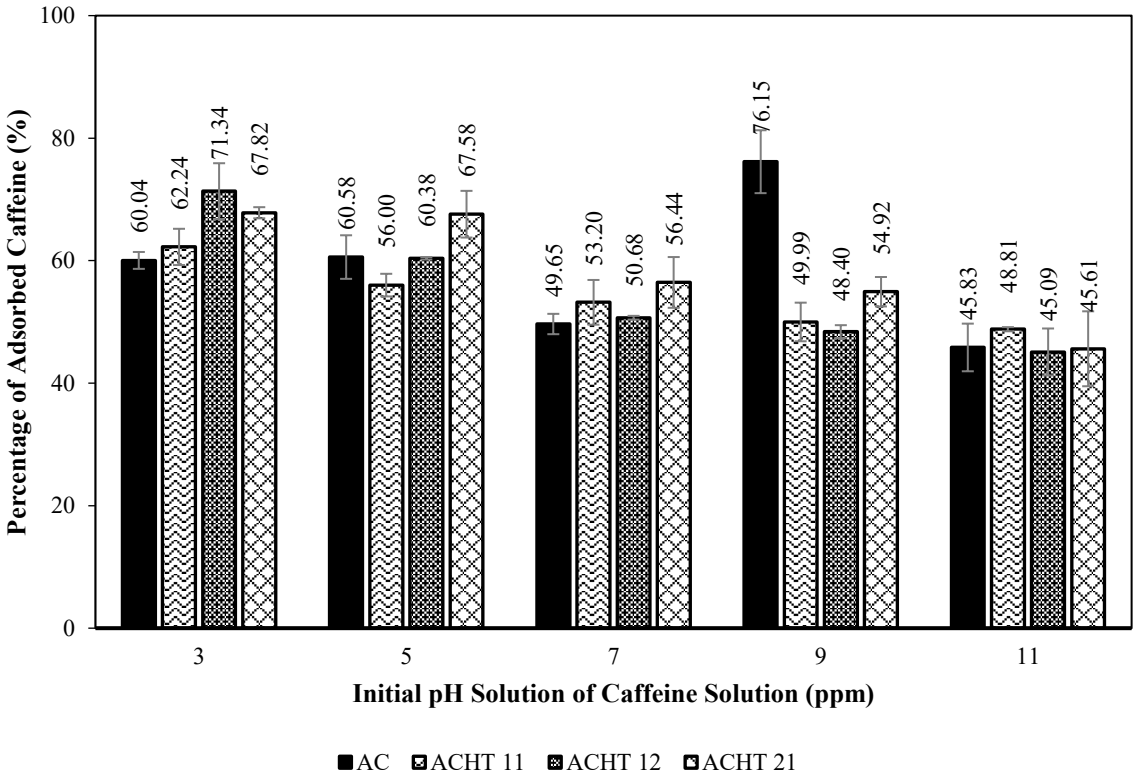

Figure 6. Effect of initial pH on the percentage of caffeine adsorbed by various adsorbents.

In contrast, ACHT 11, ACHT 12, and ACHT 21 exhibit behavior typical of positively charged HT, with *pHpzc* values usually ranging from 8 to 9. At acidic pH, the HT material surface is highly protonated, which enhances electrostatic attraction and hydrogen bonding with neutral caffeine molecules. As pH increases, the zeta potential gradually decreases and eventually becomes negative once it surpasses the pH_{pzc}, thereby weakening electrostatic interactions and allowing hydroxide ions to compete with caffeine molecules for active sites. Under fundamental conditions (pH 9 or higher), partial dissolution and structural degradation of the HT layers may occur, reducing the number of available adsorption sites. This phenomenon is consistent with recent studies on ACHT composites, which report that greater adsorption efficiency at lower pH values is attributed to dominant electrostatic and ion-exchange mechanisms [85,86].

3.6. Adsorbent Regeneration and Reusability

The caffeine adsorption performance was clearly different between AC and all ACHT samples, and this difference was affected by the number of use cycles (Figure 7). In the first cycle, ACHT 11 and ACHT 12 showed higher percentages of adsorbed caffeine (64.19% and 41.80%) than AC (41.44%), while ACHT 21 showed a value comparable to AC (40.08%). This indicates that surface modification can increase the initial affinity for caffeine. The improvement in adsorption performance was more pronounced in the second cycle, where ACHT 21 showed the highest value of 92.21%, followed by ACHT 11 (83.58%) and ACHT 12 (62.55%), while AC reached only 30.94%. The superior performance of ACHT (especially ACHT 21) can be attributed to its more open pore structure and larger pore volume, as shown in Table 2, which supports higher diffusivity and more effective utilization of internal adsorption sites. However, in the third cycle, all materials experienced a significant decrease in adsorption capacity, with the

lowest values in ACHT 21 (4.77%) and ACHT 11 (6.92%), indicating saturation of active sites and limited adsorbent regeneration. Nevertheless, ACHT 12 still showed a relatively higher adsorption (15.67%) than other samples, indicating better adsorption stability upon repeated use. These data confirm that converting AC to ACHT can improve the adsorption performance of caffeine, especially during the initial cycle. The combination of pore volume and mesoporous structure plays a more dominant role than the specific surface area alone in determining the adsorption efficiency of caffeine.

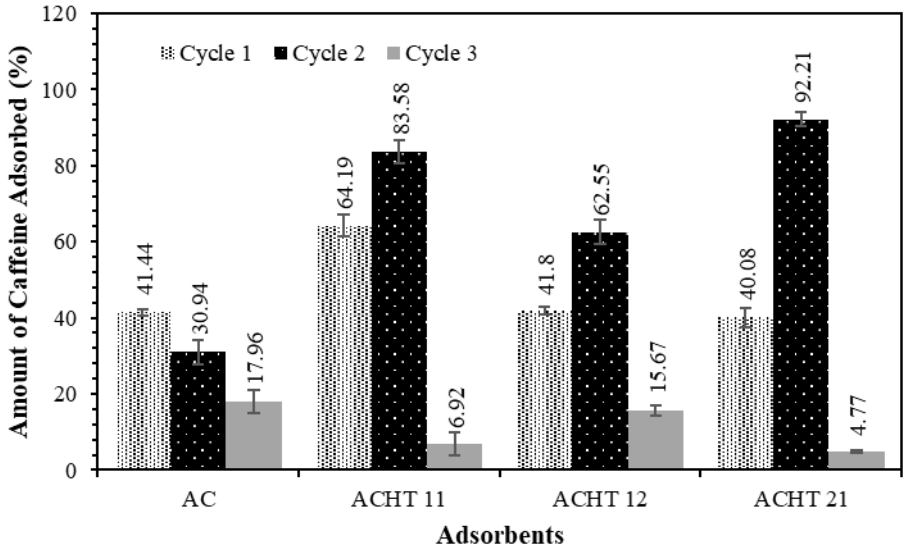

Figure 7. Effect of adsorption–desorption cycles on caffeine removal efficiency of AC, ACHT 11, ACHT 12, and ACHT 21 adsorbents.

3.7. Environmental Implications and Applicability

The utilization of jengkol peel husk biomass as a precursor for adsorbent materials presents an environmentally friendly and sustainable approach to tackling organic contaminants such as caffeine. Jengkol peel, an agricultural waste commonly discarded and contributing to organic pollution, can be transformed into high-value functional materials through activation and intercalation with HT structures. From an environmental perspective, this strategy aligns with the principles of integrated waste management, particularly by transforming waste into resources. The activation and HT composite synthesis processes employed are relatively low in energy demand and use relatively benign chemicals, minimizing residual waste and emissions. Moreover, the valorization of local biomass supports circular economy principles and contributes to Sustainable Development Goal (SDG) 6.3.

In terms of applicability, the developed adsorbent materials demonstrated considerable caffeine removal efficiency, especially at lower pH values and initial concentrations, conditions that are reflective of real pharmaceutical wastewater. Notably, the ACHT 12 and ACHT 21 composites exhibited both favorable adsorption capacities and structural stability, making them promising candidates for scalable and sustainable applications.

Furthermore, HT-based adsorbents are known for their regenerability and reusability, enabling multiple adsorption-desorption cycles, which significantly reduces material replacement frequency and operational costs. Nevertheless, further studies are warranted to assess their performance in more complex wastewater matrices, interference from competing solutes, and efficiency under continuous flow systems or pilot-scale column reactors.

4. CONCLUSION

This study demonstrated that activated carbon derived from jengkol peel (AC) and its composites with HT (ACHT 11, ACHT 12, and ACHT 21) are effective in adsorbing caffeine from aqueous solutions. AC exhibited the highest efficiency at low concentrations (up to 96.44% at 3 ppm), while the ACHT 12 composite showed competitive adsorption capacity and greater stability at moderate concentrations, with a strong fit to the Langmuir isotherm model (R^2 = 0.9609) and pseudo-second-order kinetics (R^2 = 0.9912). The ACHT 21 composite tended to follow the Freundlich model (R^2 = 0.7758), suggesting a more heterogeneous surface. Moreover, the composite adsorbents performed well under acidic pH conditions (pH 3–5), which are relevant to pharmaceutical wastewater profiles. These findings suggest that combining AC with HT, particularly at a 1:2 ratio, can enhance adsorbent–adsorbate interactions and offer a sustainable pathway for utilizing local biomass waste as eco-friendly materials for water purification.

ACKNOWLEDGMENT

The authors gratefully acknowledge the Ministry of Higher Education, Science, and Technology of the Republic of Indonesia for funding support through the Beginner Lecturer Research Grant for Fiscal Year 2025. This research was conducted under contract number: 02/LIT-DPPM/LP3M/VI/2025. The authors also thank the Research and Community Service Institute of Universitas Muhammadiyah Tasikmalaya for providing research facilities and administrative assistance.

REFERENCES

1. V. Roveri, L.L. Guimarães, W. Toma, A.T. Correia, Occurrence, Ecological Risk Assessment and Prioritization of Pharmaceuticals and Abuse Drugs in Estuarine Waters Along the São Paulo Coast, Brazil, Environ. Sci. Pollut. Res. 29 (2022) 89712–89726.
2. W. Thanasoponkul, T. Changbunjong, R. Sukkurd, T. Saiwichai, Spent Coffee Grounds and Novaluron Are Toxic to *Aedes Aegypti* (Diptera: Culicidae) Larvae, Insects 14 (2023) 564.
3. K.T. Peter, F. Hou, Z. Tian, C.L. Wu, M. Goehring, F. Liu, E.P. Kolodziej, More Than a First Flush: Urban Creek Storm Hydrographs Demonstrate Broad Contaminant Pollutographs, Environ. Sci. Technol. 54 (2020) 6152–6165.
4. S. Zheng, M. Xiao, L. Wang, Y. Li, W. Xiao, D. Xu, J. Cai, Effects of Rural Domestic Sewage Reclaimed Irrigation and Regulation on Heavy Metals, PPCPs, Water and Nitrogen Utilization, and Microbial Diversity in Paddy Field, Int. J. Agric. Biol. Eng. 16 (2023) 245–256.
5. L. Wan, L. Huang, P. Chen, Caffeine Citrate Maintenance Doses Effect on Extubation and Apnea Postventilation in Preterm Infants, Pediatr. Pulmonol. 55 (2020) 2635–2640.
6. O.S. Arvaniti, G. Gkotsis, M. Nika, S. Gyparakis, T. Manios, N.S. Thomaidis, M.S. Fountoulakis, A.S. Stasinakis, Study on the Occurrence of Artificial Sweeteners, Parabens, and Other Emerging Contaminants in Hospital Wastewater Using LC-QToF-MS Target Screening Approach, Water (Basel). 15 (2023) 936.
7. R. Muangmora, P. Kemacheevakul, P. Punyapalakul, S. Chuangchote, Enhanced Photocatalytic Degradation of Caffeine Using Titanium Dioxide Photocatalyst Immobilized on Circular Glass Sheets Under Ultraviolet C Irradiation, Catalysts 10 (2020) 964.
8. P. Paíga, L. Correia-Sá, M. Correia, S.A. Figueiredo, J. Vieira, S. Jorge, J.G. Silva, C. Delerue-Matos, Temporal Analysis of Pharmaceuticals as Emerging Contaminants in Surface Water and Wastewater Samples: A Case Study, J. Xenobiotics 14 (2024) 873–892.
9. N. Liu, X. Jin, Y. Zheng, Y. Luo, C. Feng, Z. Fu, Z. Tang, F. Wu, J.P. Giesy,

Occurrence and Multiple-Level Ecological Risk Assessment of Pharmaceuticals and Personal Care Products (PPCPs) in Two Shallow Lakes of China, Environ. Sci. Eur. 32 (2020) 69.
10. J.A. Quintero-Jaramillo, J. Carrero-Mantilla, N.R. Sanabria-González, Caffeine Adsorption on a Thermally Modified Bentonite: Adsorbent Characterization, Experimental Design, Equilibrium and Kinetics, Colloids and Interfaces 8 (2024) 26.
11. N.A. Tawfik, Z.A. El-Bakary, K.F.A. El-Wakeil, Determination of Caffeine in Treated Wastewater Discharged in the Nile River with Emphasis on the Effect of Zinc and Physicochemical Factors, Environ. Sci. Pollut. Res. 31 (2024) 28124–28138.
12. E. Jara-Negrete, I. Cipriani-Ávila, J. Molinero, V. Pinos-Vélez, S. Acosta-López, M. Cabrera, E.J. Medina-Villamizar, D. Leiva-Andrade, A. Pozo, O. Martínez, N.G. Mogollón, Pharmaceutical Compounds in Urban Drinking Waters of Ecuador, Front. Environ. Sci. 11 (2023) 1232405.
13. L. Molnárová, T. Halešová, D. Tomešová, M. Václavíková, Z. Bosáková, Monitoring Pharmaceuticals and Personal Care Products in Healthcare Effluent Wastewater Samples and the Effectiveness of Drug Removal in Wastewater Treatment Plants Using the UHPLC-MS/MS Method, Molecules 29 (2024) 1480.
14. O.F. Becerra-Rueda, G.M. Rodríguez-Figueroa, A.J. Marmolejo-Rodríguez, S. Aguíñiga-García, J.C. Durán–Álvarez, Pharmaceutical Residues in Sediments of a Coastal Lagoon in Northwest Mexico—Occurrence and Environmental Risk Assessment, J. Xenobiotics 14 (2024) 1757–1770.
15. A. Almeida, J.C.C. de Oliveira, F. Matias, C.A.Á.S. Ribeiro, D.D. Silveira, J.M.R. Tavares, Removal of Emergent Pollutants by a Vertical Flow Constructed Wetland with Vetiveria Zizanioides: A Case Study for Caffeine, KnE Mater. Sci. 7 (2022) 184–192.
16. M.M. Marshall, G.K. Metzner, K.E. McCluney, Caffeine and Canopy Cover Interact to Alter Biofilm Nutrient Content, Benthic Invertebrates, and Insect Emergence, River Res. Appl. 38 (2022) 863–872.
17. A. Woziwodzka, M. Krychowiak-Maśnicka, G. Gołuński, A. Łosiewska, A. Borowik, D. Wyrzykowski, J. Piosik, New Life of an Old Drug: Caffeine as a Modulator of Antibacterial Activity of Commonly Used Antibiotics, Pharmaceuticals 15 (2022) 872.
18. D.T.T. Quyen, M. Otaki, Y. Otaki, C. Tushara, I.W. Sanjeewa, Pharmaceutical Contaminants in Shallow Groundwater and Their Implication for Poor Sanitation Facilities in Low-Income Countries, Environ. Toxicol. Chem. 41 (2021) 266–274.
19. A. Lee, R.W. Cheng, J. Heslar, Determining the Impact of Caffeine on Aggression in Betta Splendens, J. Emerg. Invest. 7 (2024) 1–5.
20. J.E. Choi, S.-H. Heo, W. Chung, Yap1-Mediated Flr1 Expression Reveals Crosstalk Between Oxidative Stress Signaling and Caffeine Resistance in *Saccharomyces Cerevisiae*, Front. Microbiol. 13 (2022) 1026780.
21. J.S. Baron, T. Weinmann, V.K. Acharya, C. Charlton, K.R. Nydick, S.M. Esser, Marmots Do Not Drink Coffee: Human Urine Contributions to the Nitrogen Budget of a Popular National Park Destination, Ecosphere 14 (2023) e4504.
22. K.S. Obayomi, Z. Xie, S. Gray, J. Zhang, Assessing the Performance of Different Treatment Methods in Removing Tetracycline from Wastewater: Efficiency and Cost Evaluation, Materials 18 (2025) 2134.
23. Y. Kuang, X. Zhang, S. Zhou, Adsorption of methylene blue in water onto activated carbon by surfactant

modification, Water (Switzerland) 12 (2020) 587.
24. A. Saputra, O. Rina, R. Hidayat, M. Fitria, S.A. Akhni, A. Purnomo, A. Haryadi, Synthesis of Bamboo-Based Activated Carbon Through Physico-Chemical Activation for Coal-Runoff Wastewater Treatment, Indonesian J. Chem. Anal. (IJCA) 6 (2023) 143–150.
25. A.N. Kassob, A.H. Abbar, Treatment of Petroleum Refinery Wastewater by Adsorption Using Activated Carbon Fixed Bed Column With Batch Recirculation Mode, Al-Qadisiyah J. Eng. Sci. 15 (2022) 101–111.
26. Y. Hung, A.S.P. Pamula, H.H. Paul, Treatment of Combined Acid Black 48 and Coffee Wastewater by Low-Cost Adsorbents, Environ. Res. Eng. Manag. 76 (2020) 47–61.
27. F. Gao, X. Xu, J. Yang, Removal of p-Nitrophenol from Simulated Sewage Using MgCo-3D Hydrotalcite Nanospheres: Capability and Mechanism, RSC Adv. 12 (2022) 27044–27054.
28. S. Marković, V. Tomašević, Management of Waste Biomass from Food Industry: Potential Application of Peach Shells for Waste Water Treatment, Serbian J. Eng. Manag. 7 (2022) 13–21.
29. G. Bahman, H. Yazdian, Developing a Water, Food, Energy, Economy, and Environment Nexus Index for Evaluating Centralized and Decentralized Wastewater Treatment Systems, Environ. Qual. Manag. 34 (2024) e22344.
30. S. Igoud, D. Zeriri, L. Aoudjit, B. Boutra, S. Sebti, F. Khene, A. Mameche, Climate Change Adaptation by Solar Wastewater Treatment (SOWAT) for Reuse in Agriculture and Industry, Irrig. Drain. 70 (2020) 243–253.
31. D. Milićević, M. Milićević, R. Trajković, Decentralized Wastewater Treatment - A Sustainable Solution for Protecting Water Resources from Pollution, J. Fac. Civ. Eng. Archit. 39 (2024) 35–46.
32. R.E. Haraki, A.A. Arie, R.F. Susanti, H.S. Oktaviano, A. Nugroho, Synthesis and Electrochemical Properties of ZnO/ Activated Carbon from Vetiver Distillation Waste, Eng. Chem. 2 (2023) 35–41.
33. M. Ravi, S.K. Rathore, S. Murugan, Biomass-Based Activated Carbon for CO_2 Adsorption–A Review, Energy Environ. 34 (2022) 1674–1721.
34. N.B.F. de Aquino, D.B. de Morais, A.C. de Aquino, G. V Barbosa, A.A. Cavalheiro, Thermal Stability Changing Caused by Chromium (III) in the Carbonated Magnesium-Aluminum Hydrotalcite, J. Eng. Exact Sci. 6 (2020) 709–716.
35. A.P. Tathod, B. Saini, S. Arumugam, N. Viswanadham, Hybrid Nanocomposite Comprising Mg–Al Hydrotalcite Nanocrystals on ZSM-5 Zeolite for Production of Renewable Fuel Additives from Furfural, ACS Appl. Nano Mater. 6 (2023) 3580–3589.
36. W. Sun, T. Gao, G. Zhu, Q. Cao, W. Fang, Influence of Support Properties and Particle Size on the Gold-Catalyzed Base-Free Aerobic Oxidation of 5-Hydroxymethylfurfural, ChemistrySelect 5 (2020) 1416–1423.
37. A. Khalil, M.A. Salem, S. Ragab, M. Sillanpää, A.E. Nemr, Orange Peels Magnetic Activate Carbon (MG-OPAC) Composite Formation for Toxic Chromium Absorption from Wastewater, Sci. Rep. 13 (2023) 3402.
38. F. Ahmed, G. Almutairi, P.M.Z. Hasan, S. Rehman, S. Kumar, N.M. Shaalan, A. Aljaafari, A. Alshoaibi, B. AlOtaibi, K. Khan, Fabrication of a Biomass-Derived Activated Carbon-Based Anode for High-Performance Li-Ion Batteries, Micromachines (Basel). 14 (2023) 192.
39. A.A. Firdaus, E. Purwandari, R. Asih, A. Sholih, D. Darminto, Study on Optical Energy Gap and the Thickness of Boron Doped Graphenic Carbon (B-

GC) Film Prepared by Nanospray Method, Mater. Sci. Forum 1094 (2023) 123–128.
40. O.P. Gbenebor, O.A. Olanrewaju, M.A. Usman, S.O. Adeosun, Lignin from Brewers' Spent Grain: Structural and Thermal Evaluations, Polymers (Basel). 15 (2023) 2346.
41. M.S. Yerdauletov, K. Nazarov, B. Mukhametuly, M.A. Yeleuov, C. Daulbayev, R. Abdulkarimova, A. Yskakov, F. Napolskiy, V. Krivchenko, Characterization of Activated Carbon from Rice Husk for Enhanced Energy Storage Devices, Molecules 28 (2023) 5818.
42. S.K. Shahcheragh, M.M.B. Mohagheghi, A. Shirpay, Effect of Physical and Chemical Activation Methods on the Structure, Optical Absorbance, Band Gap and Urbach Energy of Porous Activated Carbon, SN Appl. Sci. 5 (2023) 313.
43. T.N. Nguyen, Q.T. Phung, Z. Yu, L. Frederickx, D. Jacques, D. Sakellariou, A. Dauzeres, J. Elsen, Y. Pontikes, Alteration in Molecular Structure of Alkali Activated Slag with Various Water to Binder Ratios under Accelerated Carbonation, Sci. Rep. 12 (2022) 5524.
44. A. Michalik, B.D. Napruszewska, A. Walczyk, J. Kryściak-Czerwenka, D. Duraczyńska, E.M. Serwicka, Synthesis of Nanocrystalline Mg-Al Hydrotalcites in the Presence of Starch—the Effect on Structure and Composition, Materials 13 (2020) 602.
45. S. Sripada, S. Vasefi, J.R. Kastner, Plasma-Activated Solid Base Carbon Monolith Catalyst for Continuous Synthesis of High-Density Aviation Fuel Precursors, Ind. Eng. Chem. Res. 63 (2024) 11413–11422.
46. Y. Zuo, Thermodynamic Modeling of the Phase Evolution in Alkali-activated Slag Cements with Sulfate Salt Exposure, J. Am. Ceram. Soc. 105 (2022) 7658–7675.
47. B. Walkley, X. Ke, J.L. Provis, S.A. Bernal, Activator Anion Influences the Nanostructure of Alkali-Activated Slag Cements, J. Phys. Chem. C 125 (2021) 20727–20739.
48. C. Foster, S. Shaw, T.S. Neill, N. Bryan, N. Sherriff, L.S. Natrajan, H. Wilson, L. Lopez-Odriozola, B. Rigby, S.J. Haigh, Y. Zou, R.W. Harrison, K. Morris, Hydrotalcite Colloidal Stability and Interactions with Uranium(VI) at Neutral to Alkaline pH, Langmuir 38 (2022) 2576–2589.
49. M. Zhang, Z. Lu, J. Zhao, Y. Hasebe, Z. Zhang, Y. Wang, Simultaneous Electrochemical Determination of Hydroquinone and Catechol by Lignocellulose Biopolymers Derived Porous Carbon, ChemistrySelect 8 (2023) e202303610.
50. Y.A. Alassmy, P.J. Paalman, P.P. Pescarmona, One-pot Fixation of CO_2 into Glycerol Carbonate Using Ion-Exchanged Amberlite Resin Beads as Efficient Metal-free Heterogeneous Catalysts, ChemCatChem 13 (2020) 475–486.
51. K.L. Chin, C.L. Lee, P.S. H'ng, U. Rashid, P.M. Tahir, P.S. Khoo, M. Mamiński, Refining Micropore Capacity of Activated Carbon Derived from Coconut Shell via Deashing Post-Treatment, Bioresources 15 (2020) 7749–7769.
52. H. Zhou, D. Lan, X. Hua, T. Deng, X. Wang, The Addition of a Small Dose of *Cinnamomum camphora* Biomass Unexpectedly Enhanced Lignocellulose Degradation During the Compost of *Stropharia rugosoannulata* Cultivation Materials, Sustainability 15 (2023) 10483.
53. W. Li, Y. Xu, G. Wang, T. Xu, K. Wang, S. Zhai, C. Si, Sustainable Carbon-Based Catalyst Materials Derived from Lignocellulosic Biomass for Energy Storage and Conversion: Atomic Modulation and Properties Improvement, Carbon Energy 7 (2025) e708.

54. Q. Yang, H. Zhou, P. Bartocci, F. Fantozzi, O. Mašek, F.A. Agblevor, Z. Wei, H. Yang, H. Chen, X. Lu, G.Q. Chen, C. Zheng, C. Nielsen, M.B. McElroy, Prospective Contributions of Biomass Pyrolysis to China's 2050 Carbon Reduction and Renewable Energy Goals, Nat. Commun. 12 (2021) 1698.
55. D.N.K.P. Negara, T.G.T. Nindhia, L. Lusiana, I.M. Astika, C.I.P.K. Kencanawati, Development and Characterization of Activated Carbons Derived from Lignocellulosic Material, Materi. Sci. Forum 988 (2020) 80–86.
56. Y. Zhu, T. Qiu, T. Liu, C. Li, Y. Huai, W. Ge, Simulation of Gas Diffusion-Adsorption Coupling in Adsorbents for Optimizing Pore Structures, Ind. Eng. Chem. Res. 63 (2024) 17402–17412.
57. S. Balou, I. Ahmed, A. Priye, From Waste to Filament: Development of Biomass-Derived Activated Carbon-Reinforced PETG Composites for Sustainable 3D Printing, ACS Sustain. Chem. Eng. 11 (2023) 12667–12676.
58. M.S. Hafizuddin, C.L. Lee, K.L. Chin, P.S. H'ng, P.S. Khoo, U. Rashid, Fabrication of Highly Microporous Structure Activated Carbon via Surface Modification with Sodium Hydroxide, Polymers (Basel). 13 (2021) 3954.
59. M. Baikousi, A. Gantzoudi, C. Gioti, D. Moschovas, A.E. Giannakas, A. Avgeropoulos, C.E. Salmas, M.A. Karakassides, Hydrogen Sulfide Removal via Sorption Process on Activated Carbon–Metal Oxide Composites Derived from Different Biomass Sources, Molecules 28 (2023) 7418.
60. A. Saha, T. Sharabani, E. Evenstein, G.D. Nessim, M. Noked, R. Sharma, Probing Electrochemical Behaviour of Lignocellulosic, Orange Peel Derived Hard Carbon as Anode for Sodium Ion Battery, J. Electrochem. Soc. 167 (2020) 90505.
61. L. Wang, X. Ma, Z. Ma, P. Li, L. Zhang, $KHCO_3$ Chemical-Activated Hydrothermal Porous Carbon Derived from Sugarcane Bagasse for Supercapacitor Applications, Chem. Asian J. (2024) e202400530.
62. M. Hasanpour, Microcrystalline Cellulose/Graphene Oxide Aerogel for Adsorption of Cationic Dye from Aqueous Solution, Mater. Sci. Technol. 39 (2023) 2730–2742.
63. O.P. Murphy, M. Vashishtha, P. Palanisamy, K.V. Kumar, A Review on the Adsorption Isotherms and Design Calculations for the Optimization of Adsorbent Mass and Contact Time, ACS Omega 8 (2023) 17407–17430.
64. J. Li, B. Li, C. Ren, K. Yang, Y. Zhang, Characterization of Methane Adsorption Behavior on Wet Shale under Different Temperature Conditions, Energy Fuels 34 (2020) 2832–2848.
65. K. Hu, H. Mischo, Absolute Adsorption and Adsorbed Volume Modeling for Supercritical Methane Adsorption on Shale, Adsorption 28 (2022) 27–39.
66. M. Beydaghdari, F.H. Saboor, A. Babapoor, V.V. Karve, M. Asgari, Recent Advances in MOF-Based Adsorbents for Dye Removal from the Aquatic Environment, Energies (Basel). 15 (2022) 2023.
67. P. Zawadzki, E. Kudlek, M. Dudziak, Titanium(IV) Oxide Modified with Activated Carbon and Ultrasounds for Caffeine Photodegradation: Adsorption Isotherm and Kinetics Study, J. Ecol. Eng. 21 (2020) 137–145.
68. R.M. Alharbi, E.N. Sholkamy, K.I. Alsamhary, N. Abdel-Raouf, I.B.M. Ibraheem, Optimization Study of the Capacity of *Chlorella vulgaris* as a Potential Bio-Remediator for the Bio-Adsorption of Arsenic (III) from Aquatic Environments, Toxics 11 (2023) 439.
69. Y. Zhao, H. Yang, J. Sun, Y. Zhang, S. Xia, Enhanced Adsorption of Rhodamine B on Modified Oil-Based Drill Cutting Ash: Characterization, Adsorption Kinetics, and Adsorption

Isotherm, ACS Omega 6 (2021) 17086–17094.
70. P.K. Obulapuram, T. Arfin, F. Mohammad, S.K. Khiste, M. Chavali, A.N. Albalawi, H.A. Al-Lohedan, Adsorption, Equilibrium Isotherm, and Thermodynamic Studies Towards the Removal of Reactive Orange 16 Dye Using Cu(I)-Polyaninile Composite, Polymers (Basel) 13 (2021) 3490.
71. D. Dutta, J.P. Borah, A. Puzari, Iron Oxide Coated Hollow Poly(methylmethacrylate) as an Efficient Adsorption Media for Removal of Arsenic from Water, RSC Adv. 11 (2021) 13376–13385.
72. E. Kianfar, H. Sayadi, Recent Advances in Properties and Applications of Nanoporous Materials and Porous Carbons, Carbon Lett. 32 (2022) 1645–1669.
73. K. Szewczuk-Karpisz, A. Tomczyk, M. Celińska, Z. Sokołowska, M. Kuśmierz, Carboxin and Diuron Adsorption Mechanism on Sunflower Husks Biochar and Goethite in the Single/Mixed Pesticide Solutions, Materials 14 (2021) 2584.
74. Y. Zhu, H. Liang, R. Yu, G. Hu, F. Chen, Removal of Aquatic Cadmium Ions using Thiourea Modified Poplar Biochar, Water (Switzerland) 12 (2020) 1117.
75. Y. Liu, W. Gao, R. Liu, W. Zhang, J. Niu, X. Lou, G. Li, H. Liu, Z. Li, Removal of Phosphorus using Biochar Derived from Fenton Sludge: Mechanism and Performance Insights, Water Environ. Res. 94 (2022) e10763.
76. B. Ashour, S.M. Ali, M.G. Farahat, R.M. El-Sherif, Fabrication and Detection of Carbon-based Nanomaterials Derived from Biomass Sources: Processes and Applications, Egypt. J. Chem. 68 (2025) 117–129.
77. A. Mokhati, O. Benturki, A. Benturki, R. Fennouh, Z. Kecira, M. Bernardo, I. Matos, N. Lapa, M. Ventura, O.S.G.P. Soares, A.M.B. Do Rego, I. Fonseca, Conversion of Argan Nutshells into Novel Porous Carbons in the Scope of Circular Economy: Adsorption Performance of Emerging Contaminants, Appl. Sci. 12 (2022) 7607.
78. Y. Sun, X.L. Shi, Y.L. Yang, G. Suo, L. Zhang, S. Lu, Z.G. Chen, Biomass-Derived Carbon for High-Performance Batteries: From Structure to Properties, Adv. Funct. Mater. 32 (2022) 2201584.
79. S. Saeki, Empirical Determination of the Helmholtz Free Energy and the Gibbs Free Energy of Polyethylene Based on the Pressure–Volume–Temperature–Entropy Equation of State and the Partition Function, J. Macromol. Sci. Part B Phys. 62 (2023) 311–328.
80. Y.S. Reddy, T.J. Jose, B. Dinesh, R.N. Kumar, P.S. Kumar, K. Kaviyarasu, Equilibrium, Kinetic, and Thermodynamic Study of Direct Yellow 12 Dye Adsorption by Biomass-Derived Porous Graphitic Activated Carbon, Biomass Convers. Biorefinery 15 (2025) 6817–6833.
81. S.D. Erkal, N. Kanmaz, P. Demircivi, Biomass Supported Magnesium-Aluminium Layered Double Hydroxide Composites as Sustainable Adsorbents for Doxycycline Removal, J. Indian Chem. Soc. 102 (2025) 101987.
82. E.N. Oliveira, A.T. Meneses, S.F. de Melo, F.M.R. Dias, M.T.B. Perazzini, H. Perazzini, L. Meili, J.I. Soletti, S.H.V. Carvalho, M.D. Bispo, Highly Effective Adsorption of Caffeine by A Novel Activated Carbon Prepared from Coconut Leaf, Environ. Sci. Pollut. Res. 29 (2022) 50661–50674.
83. F.M.O. Medina, M.B. Aguiar, M.E. Parolo, M.J. Avena, Insights of Competitive Adsorption on Activated Carbon of Binary Caffeine and Diclofenac Solutions, J. Environ. Manage. 278 (2021) 111523.
84. J.A. Quintero-Jaramillo, J.I. Carrero-Mantilla, N.R. Sanabria-González, A Review of Caffeine Adsorption Studies onto Various Types of Adsorbents, Sci. World J. 2021 (2021) 998924.

85. Y. Sun, Z. Wang, S. Zhang, C. Liu, Y. Xu, Preparation of Composites with MgAl-LDH-Modified Commercial Activated Carbon for the Quick Removal of Cr(VI) from Aqueous Solutions, Environ. Sci. Pollut. Res. 31 (2024) 41032–41045.
86. N. Niedbut, S. Bosoy, S. Intachai, P. Sumanatrakul, P. Kongsune, N. Juntarachat, N. Khaorapapong, Multifunctional Magnetic Composite: MgAl-Layered Double Hydroxide, Activated Carbon and Magnetite on Removing Both Different Charged-Dyes, Chem. Eng. Sci. 287 (2024) 119783.